# Lyapunov instability of dense Lennard-Jones fluids

H. A. Posch

*Institute for Experimental Physics, University of Vienna, Boltzmanngasse 5, A-1090 Vienna, Austria*

W. G. Hoover

*Department of Applied Science, University of California, at Davis–Livermore,*
*and Lawrence Livermore National Laboratory, University of California, Livermore, California 94550*

We present calculations of the full spectra of Lyapunov exponents for 8- and 32-particle systems in three dimensions with periodic boundary conditions and interacting with the repulsive part of a Lennard-Jones potential. A new algorithm is discussed which incorporates ideas from control theory and constrained nonequilibrium molecular dynamics. Equilibrium and nonequilibrium steady states are examined. The latter are generated by the application of an external field $\mathbf{F}_e$ through which equal numbers of particles are accelerated in opposite directions, and by thermostatting the system using Nosé-Hoover or Gauss mechanics. In equilibrium ($\mathbf{F}_e = 0$) the Lyapunov spectra are symmetrical and may be understood in terms of a simple Debye model for vibrational modes in solids. For nonequilibrium steady states ($\mathbf{F}_e \neq 0$) the Lyapunov spectra are not symmetrical and indicate a collapse of the phase-space density onto an attracting fractal subspace with an associated loss in dimensionality proportional to the square of the applied field. Because of this attractor's vanishing volume in phase space and the instability of the corresponding repellor it is not possible to observe trajectories violating the second law of thermodynamics in spite of the time-reversal invariance of the equations of motion. Thus Nosé-Hoover mechanics, of which Gauss's isokinetic mechanics is a special case, resolves the reversibility paradox first stated by J. Loschmidt [Sitzungsber. kais. Akad. Wiss. Wien 2. Abt. 73, 128 (1876)] for nonequilibrium steady-state systems.

## I. INTRODUCTION

In recent years many chaotic continuous-time systems have been studied, both experimentally and by computer simulation. A useful way to characterize their stochastic properties is the spectrum of Lyapunov characteristic exponents $\{\lambda_i\}$ describing the mean exponential rates of divergence and convergence of neighboring trajectories in phase space.[1-6] For chaotic systems the largest Lyapunov exponent is positive, whereas regular motion exhibiting fixed points, limit cycles, or Kolmogorov-Arnol'd-Moser tori leads to Lyapunov exponents $\leq 0$. Furthermore, the sum of all positive Lyapunov exponents is the Kolmogorov entropy.[4-6]

For any flow in $M$-dimensional phase space described by the set of first-order differential equations,

$$\dot{\Gamma} = \mathbf{G}(\Gamma) , \tag{1.1}$$

$$\Gamma = \{x_i\} , \quad i = 1, 2, \ldots, M \tag{1.2}$$

there are $M$ Lyapunov exponents of which at least one must vanish.[6] In dissipative flows, such as the famous Lorenz model of turbulence or the Navier-Stokes equations of continuum mechanics, the phase-space volume is not conserved but shrinks, in the course of time, resulting in the appearance of a strange attractor. As a result the spectrum of Lyapunov exponents is not symmetrical around zero and the sum of all exponents is negative. Two different connections between the Lyapunov spec-

trum and the fractal dimension of the strange attractor have been conjectured by Kaplan and Yorke[7,8] and Mori.[9] However, if the flow (1.1) is derived from a Hamiltonian at constant internal energy, the spectrum of Lyapunov exponents is symmetrical around zero,

$$\lambda_i = -\lambda_{M-i+1} , \tag{1.3}$$

and two of the exponents must vanish. Any further constant of the motion (such as one component of linear momentum) causes two of the remaining Lyapunov exponents to vanish.

In this paper we are concerned with the calculation of the full Lyapunov spectrum of a system of $N$ particles interacting via a repulsive Lennard-Jones potential,

$$\phi(r) = \begin{cases} 4\varepsilon \left[ \left[ \dfrac{\sigma}{r} \right]^{12} - \left[ \dfrac{\sigma}{r} \right]^{6} \right] + \varepsilon , & r < 2^{1/6}\sigma \\ 0 , & r \geq 2^{1/6}\sigma . \end{cases} \tag{1.4}$$

The total potential energy is assumed to be pairwise additive,

$$\Phi = \sum_{i<j} \phi(r_{ij}) , \tag{1.5}$$

where $r_{ij}$ is the distance between particles $i$ and $j$. Both equilibrium and stationary nonequilibrium states are considered. Since the center-of-mass motion is conserved, there are $M = 6(N-1)$ Lyapunov exponents and

$M(M+1)$ first-order differential equations to be solved simultaneously (see Sec. III). To keep this number below a tolerable limit we treat the cases of $N=8$ and $N=32$ particles corresponding to 1806 and 34 782 differential equations, respectively. We find that in the equilibrium liquid case the Lyapunov spectra have a very simple appearance and follow a power law in agreement with a previous model calculation for a somewhat simplified interaction potential.[10,11] We defer the discussion of our results to Secs. IV and V.

The nonequilibrium situation is realized by introducing in the Hamiltonian a constant external field $F_e$ through which half of the particles are accelerated towards opposite directions. For this "color"-conductivity problem, to achieve steady-state conditions a homogeneous Gauss thermostat is used.[12-14] In this method the equations of motion of all particles are modified by the introduction of a constraint force designed to keep the kinetic energy $K$ of the system equal to a constant value $K_0$,

$$\dot{\Gamma} = \begin{cases} \dot{\mathbf{q}} = \mathbf{p}/m \\ \dot{\mathbf{p}} = \mathbf{F}(\mathbf{q}) - \zeta_G \mathbf{p} \end{cases} . \tag{1.6}$$

Here $\mathbf{q}$ and $\mathbf{p}$ are the positions and momenta of the particles, respectively,

$$\mathbf{F}(\mathbf{q}) = -\frac{\partial \Phi}{\partial \mathbf{q}} + c\mathbf{F}_e \tag{1.7}$$

is the total intrinsic force acting on a particle, and $\mathbf{F}_e$ is an external force, $c$ being $+1$ for half of the particles and $-1$ for the other half. The constraint force term $-\zeta_G \mathbf{p}$ contains a thermostat variable $\zeta_G$ identical for all particles and determined at any instant of time from

$$\zeta_G = \frac{\frac{1}{m}\sum \mathbf{F}(\mathbf{q}) \cdot \mathbf{p}}{\frac{1}{m}\sum \mathbf{p} \cdot \mathbf{p}} . \tag{1.8}$$

(To simplify the notation we omit unambiguous summation indices. Any unspecified sum in the following means a summation over all $N$ particles of the system.) In this "isokinetic" simulation the phase-space dimension and consequently the number of Lyapunov exponents is the same as in Hamiltonian mechanics ($\zeta_G \equiv 0$). Since the kinetic energy is a constant of the motion, again two of the exponents vanish in the equilibrium case ($\mathbf{F}_e = 0$) as compared to one in the nonequilibrium simulation ($\mathbf{F}_e \neq 0$). For the latter the sum of all Lyapunov exponents is found to be negative. The consequences of this important finding will be discussed in Sec. V.

An even more general modification of Hamiltonian mechanics has been recently invented by Nosé[15-17] making it possible to control independent thermodynamic variables during a simulation of a dynamical system through integral feedback both in equilibrium and nonequilibrium states.[18-22] In the formulation of Hoover[18,19,14] the equations of motion generating isothermal flow assume the form

$$\dot{\Gamma} = \begin{cases} \dot{\mathbf{q}} = \mathbf{p}/m \\ \dot{\mathbf{p}} = \mathbf{F}(\mathbf{q}) - \zeta \mathbf{p} \\ \dot{\zeta} = \frac{1}{\tau^2}\left[\frac{K}{K_0} - 1\right] \end{cases} , \tag{1.9}$$

where $\mathbf{F}(\mathbf{q})$ is given by (1.7). Because of linear momentum conservation and the inclusion of the thermostat variable $\zeta$ as an independent variable, the phase-space dimension and consequently the number of Lyapunov exponents is $6(N-1)+1$. $K = \sum \mathbf{p}^2/2m$ is the kinetic energy and $K_0 = 3NkT/2$ its long-time-averaged value. In thermostatted equilibrium ($\mathbf{F}_e = 0$) the corresponding distribution function turns out to be canonical,

$$f_\zeta = \frac{\exp[-H(\Gamma)/kT]}{\int d\Gamma \exp[-H(\Gamma)/kT]} , \tag{1.10}$$

where the internal energy of the total system (including the thermostat) is defined by

$$H(\Gamma) = K + \Phi + 3NkT\tau^2\zeta^2/2 . \tag{1.11}$$

$\tau$ is an unspecified parameter related to the response time of the thermostat. In the limit of infinitely fast response ($\tau \rightarrow 0$) Nosé's isothermal dynamics becomes indistinguishable from Gaussian isokinetic flow (1.6).

It is important to notice that both the Gauss and Nosé equations of motion are invariant with respect to time reversal. In Nosé's original Hamiltonian the friction variable $\zeta$ arises as a momentum variable and consequently changes sign in the time-reversed motion as well as the particle momenta $\mathbf{p}$, whereas the coordinates $\mathbf{q}$ and forces $\mathbf{F}(\mathbf{q})$ remain unchanged.

As a simple illustration of how Nosé mechanics works the one-dimensional problem of a particle in a constant external field $F_e$ will be treated in Sec. II. In Sec. III various methods for calculating the complete spectrum of Lyapunov exponents for many-body equilibrium and nonequilibrium systems are discussed. The results of our calculations are presented in Sec. IV and are further discussed in Sec. V.

## II. ONE-DIMENSIONAL "NOSÉ-HOOVER" DYNAMICS OF A PARTICLE IN A CONSTANT FIELD

As a simple illustration of Nosé-Hoover mechanics we consider the one-dimensional motion of a particle in a constant external field $F_e$. Since the long-time-averaged kinetic energy assumes the value $K_0 = kT/2$, where $T$ is the temperature maintained by the Nosé thermostat, the equations of motion obtained from (1.8) are

$$\dot{q} = p/m ,$$

$$\dot{p} = F_e = \zeta p , \tag{2.1}$$

$$\dot{\zeta} = \frac{1}{\tau^2}\left[\frac{p^2}{mkT} - 1\right] .$$

The friction variable $\zeta$ becomes more negative whenever energy is to be fed into the system, and more positive when energy is to be extracted. A projection of possible
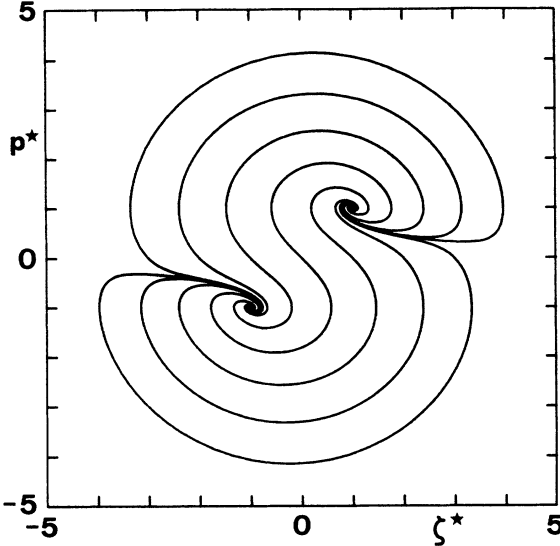
FIG. 1. Projection of the flow (2.1) onto the $p\zeta$ plane for a reduced thermostat response time $\tau F_e/\sqrt{mkT} = 1$. $p^* \equiv p/\sqrt{mkT}$ and $\zeta^* \equiv \zeta\tau$.

trajectories onto the $p\zeta$ plane is depicted in Fig. 1 for a reduced thermostat response time $\tau(F_e/\sqrt{mkT}) = 1$. The flow equations (2.1) are time reversible with $p$ and $\zeta$ replaced by $-p$ and $-\zeta$ in the time-reversed motion. This corresponds to inversion through the origin in Fig. 1. The motion in $q$ direction becomes uniform for $t \to \infty$ and is associated with a Lyapunov exponent $\lambda_1 = 0$. The stable fixed point $(\sqrt{mkT}, F_e/\sqrt{mkT})$ in $p\zeta$ space is an attractor characterized by Lyapunov exponents $\lambda_{2,3} = -F_e/2\sqrt{mkT}$ if the thermostat response time $\tau < \sqrt{8mkT}/F_e$. Time-reversal transforms this attractor into an unstable fixed point $(-\sqrt{mkT}, -F_e/\sqrt{mkT})$ which is called a repellor and which is characterized by positive Lyapunov exponents. The flow in Fig. 1 is reminiscent of a dollar sign, always leaving the vicinity of the repellor and heading for the attractor. This is true both in the original and the time-reversed case.

This simple example serves to introduce the concept of a repellor as a set obtained from an attracting set by invoking a time-reversal transformation. We shall use it in Sec. V to discuss the irreversible behavior of steady-state nonequilibrium systems.

### III. COMPUTATIONAL METHODS

Basically two algorithms for the calculation of the complete spectrum of Lyapunov exponents have been proposed.[23,24,5,2,3] In all these schemes—in addition to the reference trajectory (1.1)—$M$ further trajectories are calculated, which are differentially separated from the reference trajectory and which obey the set of linearized equations of motion obtained by differentiating (1.1),

$$\frac{d}{dt}(\delta\Gamma)_l \equiv \dot{\delta}_l = \underline{D}\cdot\delta_l , \quad l = 1, 2, \ldots, M . \tag{3.1}$$

Here, the coefficient matrix

$$\underline{D}(\Gamma) = \frac{\partial G(\Gamma)}{\partial \Gamma} \tag{3.2}$$

is an $M \times M$ matrix and couples the reference trajectory to the various differential offset vectors $\delta_l$ in "tangent space." An arbitrarily oriented set of orthonormal vectors may be chosen as initial conditions for the $M$ different vectors $\delta_l$. However, as is well established for chaotic systems, these vectors do not stay orthogonal to each other for $t > 0$ but start rotating into the direction of maximum phase-space growth and eventually diverge. To avoid this problem a Gram-Schmidt reorthonormalization procedure may be repeatedly applied to the vector frame $\{\delta_l\}$ after every few times steps.[24,5,2] In this way we obtain the results that, after some transient time, $\delta_1$ tends to point into the direction of phase space growing most rapidly proportional to $\exp(\lambda_1 t)$, that $\delta_1, \delta_2$ span a subspace whose area grows most rapidly proportional to $\exp(\lambda_1 + \lambda_2)t$, and so forth. Generally, $\delta_1, \delta_2, \ldots, \delta_l$ span a subspace with maximum volume growth proportional to $\exp(\lambda_1 + \lambda_2 + \cdots + \lambda_l)t$. From this sequence $\lambda_1, \lambda_2, \ldots, \lambda_l$ may be obtained. Most determinations of Lyapunov exponents have made use of this algorithm which we shall refer to as "method $A$."[2,5,6] As an alternative to the Gram-Schmidt reorthonormalization scheme a matrix orthogonalization technique has been proposed by Eckmann and co-workers[3] (method $B$).

We have recently introduced a third method,[10,25] henceforth referred to as "method $C$," utilizing ideas from control theory and constraint dynamics.[14] This approach has been also suggested by Goldhirsch et al.[26] Instead of allowing the linearized trajectories (3.1) to evolve freely and calculating the Lyapunov exponents by periodically rescaling the differential offset vectors $\delta_l$ in tangent space as in method $A$, these vectors may be constrained to stay normalized and orthogonal to each other at all times,

$$\delta_i^t(t)\cdot\delta_j(t) = \delta_{ij} \tag{3.3}$$

($\delta_{ij}$ is Kronecker's symbol and $t$ denotes the transpose). To achieve this, constraint "forces" must be introduced into the evolution equations (3.1),

$$\dot{\delta}_1 = \underline{D}\cdot\delta_1 - \lambda_{11}\delta_1 ,$$
$$\dot{\delta}_2 = \underline{D}\cdot\delta_2 - \lambda_{21}\delta_1 - \lambda_{22}\delta_2 ,$$
$$\vdots \tag{3.4}$$
$$\dot{\delta}_M = \underline{D}\cdot\delta_M - \lambda_{M1}\delta_1 - \lambda_{M2}\delta_2 - \cdots - \lambda_{MM}\delta_M .$$

The magnitude of the constraint forces is governed by Lagrange multipliers $\lambda_{ij}$ which may be calculated from the requirements (3.3). For example, differentiating (3.3) for $i = j$, we find

$$\delta_i^t\cdot\dot{\delta}_i = 0 .$$

Insertion of $\dot{\delta}_i$ from (3.4) gives for the main diagonal elements

$$\lambda_{ii} = \delta_i^t\cdot\underline{D}\cdot\delta_i , \quad i = 1, 2, \ldots, M . \tag{3.5}$$

Similarly, we find for $i \neq j$,

$$\delta_i^t\cdot\dot{\delta}_j + \delta_j^t\cdot\dot{\delta}_i = 0$$

and

$$\lambda_{ij} = \delta_j^t \cdot \underline{D} \cdot \delta_i + \delta_i^t \cdot \underline{D} \cdot \delta_j \ . \tag{3.6}$$

The time evolution of $\delta_1, \delta_2, \ldots, \delta_M$ is a rotation in tangent space where an arbitrarily oriented set of orthonormal vectors may serve as an initial condition for the set $\{\delta_i(0)\}$. The Lyapunov exponents are given by the time-averaged diagonal elements of the Lagrange multipliers,

$$\lambda_i = \lim_{t_{max} \to \infty} \frac{1}{t_{max}} \int_0^{t_{max}} \lambda_{ii} dt \ . \tag{3.7}$$

The theoretical merits of method $C$ are that the Lyapunov exponents are evaluated directly from the evolution equations (3.4) with their symmetry properties with respect to time-reversal explicitly displayed. In this connection it is useful to recognize that the dynamical behavior of the orthonormal set $\{\delta_i\}$ is local in phase space. By this we mean that the Lagrange multipliers $\lambda_{ij}$ and consequently the angular velocities $\omega_l$ of the rotating unit vectors depend only on the instantaneous phase point $\Gamma(t)$. They may be generated by starting at $\Gamma(t)$ and integrating the reference trajectory (1.1) *backward* in time for a time interval $\Delta t$. At $t - \Delta t$ an arbitrarily oriented set of orthonormal unit vectors $\{\delta_i(t - \Delta t)\}$ may be used as initial condition for a subsequent integration *forward* in time of both (1.1) and (3.4) to find the current $\{\delta_i(t)\}$, $\lambda_{ij}$, and $\omega_l$ at $\Gamma(t)$. For large enough time intervals $\Delta t$ the result will be independent of the initial conditions for $\{\delta_i\}$ at $t - \Delta t$. The local frequencies $\omega_l$ may become useful for semiclassical path-integral methods introduced recently.[27]

There are, however, some problems in a practical implementation of method $C$. The extensive vector-matrix operations in (3.5) and (3.6) necessary at each time step decrease the calculation speed on a VAX-750 computer by a factor of 4 as compared to method $A$ for the calculation of the full Lyapunov spectrum of an 8-particle system in three-dimensions ($M = 42$). Another minor problem arises from the restricted computational accuracy. Minor deviations are magnified in the course of time resulting in a noticeable violation of condition (3.3) after a certain number of time steps. However, this can be easily remedied by a periodic application of the Gram-Schmidt reorthonormalization scheme with negligible expense in computer time.

In a practical realization of method $C$ a convenient way of performing the time averages over the Lyapunov exponents (3.7) or of any other dynamical quantities, such as the potential energy $\Phi$, is to add these quantities to the list of variables $\{\dot{\Gamma}, \delta_1, \ldots, \delta_M\}$ integrated by the integration method in use. For all our simulation results reported in Sec. IV a fourth-order Runge-Kutta integration with a reduced time step of 0.001 was employed. Reduced units with $m$, $\sigma$, and $\varepsilon$ acting as units of mass, length, and energy together with periodic boundary conditions are used. The Lyapunov spectra obtained by methods $A$ and $C$ for the 8-particle systems agreed to better than 5% if in both runs the trajectories were followed for $10^5$ time steps. It is interesting to note that in very stiff systems the off-diagonal Lagrange multipliers $\lambda_{Mi}$ associated with the most negative Lyapunov ex-

ponent $\lambda_M$ may become extremely large, making it difficult for the algorithm to keep $\delta_M$ normalized and orthogonal to all the other vectors $\delta_1, \ldots, \delta_{M-1}$. If this happens Gram-Schmidt reorthonormalization must be used every few time steps to prevent the solution for $\lambda_M$ from becoming unstable. For the 32-body fluids also reported in Sec. IV only method $A$ has been used.

## IV. LYAPUNOV SPECTRA OF 8- AND 32-BODY FLUIDS

Figure 2 shows Lyapunov spectra for three thermodynamic states of an equilibrium (isoenergetic) 8-body system obeying Hamiltonian equations of motion and periodic boundary conditions. All data are in reduced units. Only positive exponents are calculated and indicated by the symbols in this figure. The negative exponents can be easily obtained from the symmetry condition (1.3), where $M = 42$. The exponents are arranged such that the index $n = (M/2) - i$, $i = 1, 2, \ldots, M/2$ denotes the number of positive Lyapunov exponents less than or equal to a given exponent $\lambda(n)$. The spectra have a very simple appearance and do not exhibit any fine structure. They can be approximated well by a power law

$$\lambda(n) = \alpha n^\beta \ , \tag{4.1}$$

as shown by the smooth curves in Fig. 2, which are extended also to the full range of negative Lyapunov exponents. The fit parameters $\alpha$ and $\beta$ are collected in Table I together with relevant thermodynamic information on the states considered.
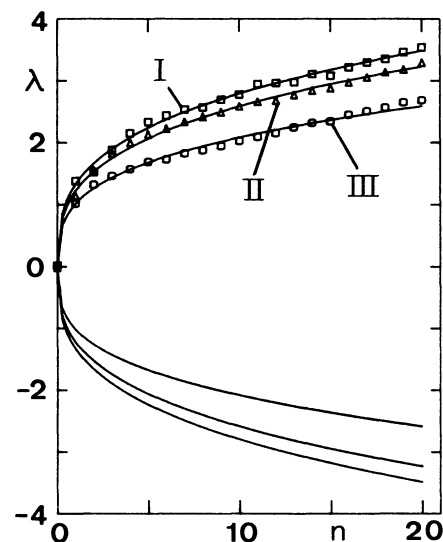


FIG. 2. Lyapunov spectra for an 8-body fluid in isoenergetic equilibrium for three thermodynamic states I, II, and III specified in Table I. Only positive exponents are calculated and indicated by the symbols. The smooth curves represent a fit of (4.1) to these data and are extended also to the full range of negative exponents. All quantities are in reduced units, with the potential parameters $\varepsilon$ and $\sigma$ of (1.4) and the mass $m$ acting as units of energy, length and mass, respectively.

TABLE I. Parameters characterizing the isoenergetic 8-body system studied in Fig. 2. All quantities are given in reduced units. $V$ is the volume, $T$ is the temperature, $K$ is the kinetic energy, $\Phi$ is the potential energy, and $E$ is the total energy. $t_{max}$ is the time for which the trajectory was followed after the decay of transients. $\alpha$ and $\beta$ are obtained by fitting (4.1) to the positive Lyapunov exponents. $\nu_D$ is an estimate for the Debye frequency, and $\lambda_{max}$ is the maximum Lyapunov exponent. $h_K = \sum_{\lambda > 0} \lambda$ is the sum over all positive exponents.

| State | I | II | III |
|---|---|---|---|
| $V$ | 16.0 | 16.0 | 22.87 |
| $kT$ | 0.85 | 0.70 | 0.684 |
| $\langle K \rangle^{a}$ | 10.20 | 8.40 | 8.21 |
| $\langle \Phi \rangle$ | 1.80 | 1.42 | 0.79 |
| $\langle E \rangle$ | 12.00 | 9.82 | 9.00 |
| $t_{max}$ | 150 | 100 | 100 |
| $\alpha$ | 1.33 | 1.22 | 1.02 |
| $\beta$ | 0.32 | 0.32 | 0.31 |
| $\nu_D$ | 3.22 | 3.03 | 3.01 |
| $\lambda_{max}$ | 3.52 | 3.30 | 2.70 |
| $h_K$ | 54.2 | 50.1 | 40.4 |

[a]The center-of-mass velocity is kept constant.

A very similar result has been found by us already for a simpler, but also purely repulsive pair potential.[10,11] Table I shows that the exponent $\beta$ is close to $\frac{1}{3}$ in all cases, which is precisely the value derived from a Debye model for the distribution of vibrational frequencies in a solid. In such a model the number of modes $dn$ between frequencies $\nu$ and $\nu + d\nu$ is proportional to $\nu^2$. Integrating this relation one finds $\lambda(n) \propto n^{1/3}$, which is of the form (4.1) with $\beta_{Debye} = \frac{1}{3}$. As may be verified from Table I, the maximum Lyapunov exponent $\lambda_{max}$ is also close in value to the Debye frequency $\nu_D$. The latter may be es-



FIG. 4. Lyapunov spectrum for an isokinetic 32-body fluid at equilibrium ($F_e = 0$). Thermodynamic state parameters are listed in Table II. Simulation results are indicated by squares, whereas the smooth line is a fit of (4.1) to the positive exponents. All quantities are in reduced units.

timated from the second derivative of the pair potential $\phi''(R)$ calculated at the particle separation $R$ for which $\phi(R) = kT$,

$$2\pi \nu_D = [\phi''(R)/m]^{1/2} . \qquad (4.2)$$

In Figs. 3–5 analogous spectra are shown for thermostatted isokinetic 8- and 32-body systems, where Gauss's equations of motion (1.6) have been applied. Let us discuss the case of field-free equilibrium first ($F_e = 0$ in Figs. 3 and 4). The power law (4.1) provides a good fit of the


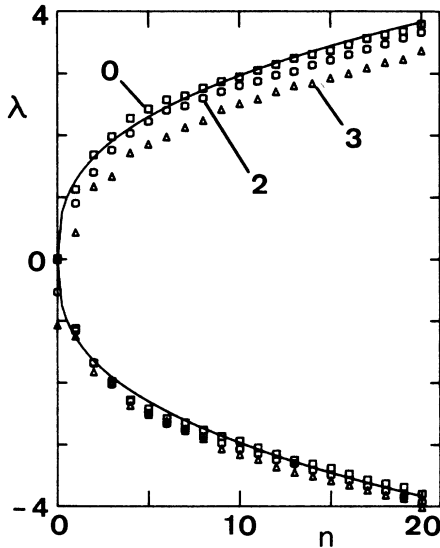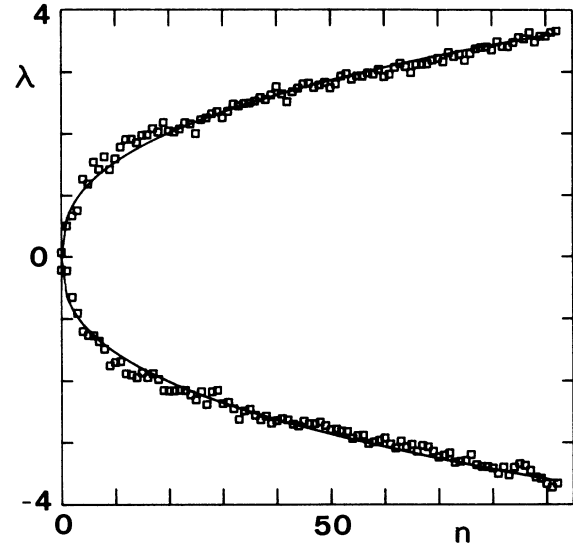
FIG. 3. Full Lyapunov spectra for an isokinetic 8-body fluid for various reduced external fields $F_e$, as indicated by the labels. The simulation results are shown as symbols, whereas the smooth line is a fit of (4.1) to the positive exponents for the equilibrium case ($F_e = 0$). Thermodynamic states and relevant parameters are listed in Table II. All quantities are in reduced units.
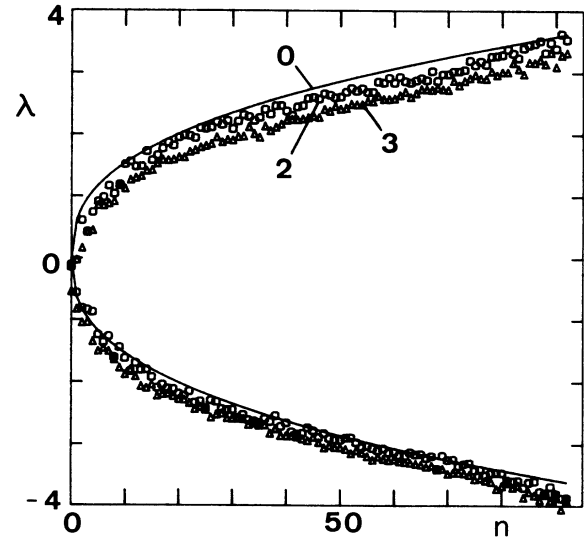


FIG. 5. Full Lyapunov spectra for an isokinetic 32-body fluid for various reduced external fields $F_e$, as indicated by the labels. The simulation results are shown as symbols. The solid curve is a fit of (4.1) to the positive exponents for the equilibrium case ($F_e = 0$) depicted in Fig. 4. Thermodynamic and related information is given in Table III. All quantities are in reduced units.

TABLE II. Parameters for the isokinetic 8-body simulations for various external fields $F_e$. All quantities are given in reduced units. In addition to the symbols explained in Table I, $d_L$ denotes the Lyapunov dimension, $\kappa$ denotes the conductivity, and $\sum\lambda$ denotes the sum over all Lyapunov exponents. $\tilde{T}$ is the "current" temperature defined in the Appendix and $\langle\Lambda\rangle$ is calculated from (5.6).

| | $F_e$ (reduced units) | | | |
| | 0.0 | 1.0 | 2.0 | 3.0 |
| --- | --- | --- | --- | --- |
| $V$ | 16.0 | 16.0 | 16.0 | 16.0 |
| $kT$ | 1.0 | 1.0 | 1.0 | 1.0 |
| $k\tilde{T}$ | 1.0 | 0.99 | 0.95 | 0.86 |
| $K_0$ [a] | 12.0 | 12.0 | 12.0 | 12.0 |
| $\langle\Phi\rangle$ | 2.21 | 2.20 | 2.22 | 1.99 |
| $\langle E\rangle$ | 14.21 | 14.20 | 14.22 | 13.99 |
| $t_{max}$ | 220 | 56 | 350 | 88 |
| $\alpha$ | 1.27 | | | |
| $\beta$ | 0.37 | | | |
| $\nu_D$ | 3.40 | | | |
| $\lambda_{max}$ | 3.79 | 3.72 | 3.67 | 3.37 |
| $h_K$ | 57.6 | 56.4 | 53.8 | 47.5 |
| $\sum\lambda$ | 0 | $-1.3$ | $-5.9$ | $-14.3$ |
| $\langle\Lambda\rangle$ | 0 | $-1.4$ | $-5.8$ | $-14.3$ |
| $d_L$ | 42 | 41.64 | 40.51 | 38.3 |
| $\kappa$ | | $0.094\pm0.013$ | $0.099\pm0.004$ | $0.108\pm0.007$ |

[a]The center-of-mass velocity is kept constant.

numerical Lyapunov spectra. The fit parameters and further relevant information for these systems are collected in Tables II and III, respectively. The exponent $\beta$ is again in quite good agreement with the Debye result $\frac{1}{3}$, and the maximum Lyapunov exponent seems to agree satisfactorily with the estimation of $\nu_D$ based on (4.2). At first the rather close agreement of the Lyapunov spectra with predictions derived from a simple Debye model is surprising. In hindsight it appears plausible in view of the fact that the coefficient matrix (3.2) is formally similar to the expansion coefficients of the potential energy $\Phi$ in powers of atomic lattice site displacements used in the theory of lattice dynamics of harmonic solids.[28] However-

er, a close inspection of Fig. 3 reveals systematic deviations of the numerically obtained points from the fit particularly at small values of $\lambda$ and $n$. These deviations also persist whether method $A$ or method $C$ is used for the simulation of the spectra. It remains to be seen whether the inclusion of an attractive part to the pair potential has a noticeable influence on the shape of the Lyapunov spectra.

Nonequilibrium steady-state results are shown in Figs. 3 and 5. As expected, the application of an external field $F_e\neq0$ destroys the symmetry of the Lyapunov spectra. They are not shifted uniformly to more negative values of $\lambda$, but the positive branch of the spectra decreases more

TABLE III. Parameters for the isokinetic 32-body simulations for various external fields $F_e$. All quantities are given in reduced units and are explained in Tables II and III.

| | $F_e$ (reduced units) | | | |
| | 0.0 | 1.0 | 2.0 | 3.0 |
| --- | --- | --- | --- | --- |
| $V$ | 64.0 | 64.0 | 64.0 | 64.0 |
| $kT$ | 1.0 | 1.0 | 1.0 | 1.0 |
| $k\tilde{T}$ | 1.0 | 0.98 | 0.94 | 0.86 |
| $K_0$ [a] | 48.0 | 48.0 | 48.00 | 48.00 |
| $\langle\Phi\rangle$ | 8.33 | 8.87 | 8.99 | 8.59 |
| $\langle E\rangle$ | 56.33 | 56.87 | 56.99 | 56.59 |
| $t_{max}$ | 5.8 | 26.0 | 10.4 | 14.0 |
| $\alpha$ | 0.634 | | | |
| $\beta$ | 0.385 | | | |
| $\nu_D$ | 3.40 | | | |
| $\lambda_{max}$ | 3.66 | 3.66 | 3.57 | 3.33 |
| $h_K$ | 242 | 238 | 225 | 203 |
| $\sum\lambda$ | 0 | $-6.8$ | $-27.1$ | $-60.8$ |
| $\langle\Lambda\rangle$ | 0 | $-6.8$ | $-27.3$ | $-60.3$ |
| $d_L$ | 186.0 | 184.2 | 178.9 | 169.8 |
| $\kappa$ | | $0.108\pm0.005$ | $0.109\pm0.005$ | $0.107\pm0.004$ |

[a]The center-of-mass velocity is kept constant.

strongly than the negative one. In Tables II and III we also list the sum over all Lyapunov exponents which is equal to the phase-space "compressibility" averaged over the nonequilibrium ensemble,

$$\langle \Lambda \rangle \equiv \int d\Gamma\, f(\Gamma, t) \frac{\partial}{\partial \Gamma} \cdot \dot{\Gamma}(\Gamma, t) = \sum_{i=1}^{M} \lambda_i \ . \tag{4.3}$$

Here, $f(\Gamma, t)$ is the distribution function obeying the general Liouville equation[29,22]

$$\frac{\partial f}{\partial t} + \frac{\partial}{\partial \Gamma} \cdot (f \dot{\Gamma}) = 0 \ . \tag{4.4}$$

Tables II and III also contain the Kolmogorov entropy $h_K$, which according to Pesin is the sum over all positive Lyapunov exponents,[30,6]

$$h_K = \sum_{\lambda > 0} \lambda \ . \tag{4.5}$$

$h_K$ is the mean rate at which information about the system is lost in the course of time.

With the external field $F_e$ applied, the system experiences also a dissipative flux in the direction of the field, the color current, defined by

$$J = \sum c\, p / m \ , \tag{4.6}$$

where $c = \pm 1$ is the color introduced in (1.7). We have measured this quantity from which a steady-state color conductivity may be derived according to

$$\langle J \rangle = V \kappa F_e \ . \tag{4.7}$$

$\kappa$ is also collected in the tables. The error bars for $\kappa$ are estimated from the numerical noise for the components of $\langle J \rangle$ perpendicular to $F_e$ which theoretically should be zero.

## V. IRREVERSIBILITY IN NONEQUILIBRIUM STEADY-STATE SYSTEMS

The internal energy of the system is defined by

$$H(\Gamma) = \Phi + \sum \frac{p^2}{2m} \ . \tag{5.1}$$

For Gaussian mechanics its rate of change is given by

$$\dot{H}(\Gamma) = \dot{\Gamma} \cdot \frac{\partial H}{\partial \Gamma} = -2K_0 \zeta_G + J(t) \cdot F_e \ , \tag{5.2}$$

where (1.6) and (1.7) have been used and J is the dissipative flux defined in (4.6). The steady-state condition $\langle \dot{H} \rangle = 0$ therefore gives

$$\langle \zeta_G \rangle = \frac{1}{2K_0} \langle J \rangle \cdot F_e = \frac{V}{2K_0} \kappa F_e^2 > 0 \ , \tag{5.3}$$

where in the second step we have used (4.7). The long-time average of $\zeta_G$ acts as a positive friction coefficient removing the energy from the system which is continuously supplied by the external field.

For the phase-space compressibility we find

$$\Lambda = \frac{\partial}{\partial \Gamma} \cdot \dot{\Gamma} = \sum \left[ \frac{\partial}{\partial q} \cdot \dot{q} + \frac{\partial}{\partial p} \cdot \dot{p} \right]$$

$$= -3(N-1)\zeta_G - \frac{1}{2K_0} \sum \left[ p \cdot \frac{\partial \Phi}{\partial q} \right]$$

$$- \frac{1}{2K_0} J \cdot F_e \ , \tag{5.4}$$

where $3(N-1)$ gives the dimension of momentum space. Upon averaging, the second term in (5.4) vanishes and we find

$$\langle \Lambda \rangle = -3(N-1)\langle \zeta_G \rangle - \frac{1}{2K_0} \langle J \rangle \cdot F_e \ . \tag{5.5}$$

Combining this equation with (5.3) yields

$$\langle \Lambda \rangle = -[3(N-1)+1] \frac{V}{2K_0} \kappa F_e^2 \ . \tag{5.6}$$

Since $\langle \Lambda \rangle$ in (4.3) is equal to the sum of all Lyapunov exponents, (5.6) provides a convenient test of the numerical consistency of the data. As indicated in the tables, we find very good agreement of $\langle \Lambda \rangle$, calculated from (5.6) with the parameters taken from Tables II and III, respectively, with $\sum \lambda$.

For nonvanishing external fields the time-averaged sum of Lyapunov exponents $\sum \lambda = \langle \Lambda \rangle$ is always negative and varies according to (5.6) with the square of the applied field. This result has extremely interesting consequences and provides an understanding of the irreversible behavior of nonequilibrium steady-state systems in spite of the time-reversal invariance of the equations of motion.[31,32] It means that an arbitrary hypervolume in phase-space centered on a trajectory *shrinks* in the course of time and develops into a very complicated fractal-like object. That systems in nonequilibrium steady states develop into "strange attractors" has been first observed in simulations of a periodic two-dimensional classical Lorentz gas driven by an external field[33] and of a single-body, one-dimensional Frenkel-Kontorova model for isothermal electronic conduction.[34] The self-similar, sheetlike structure of these fractal attractors is clearly visible for the problems mentioned above involving a phase space of only three dimensions. For the high-dimensional phase spaces treated in this paper it is obviously not possible to generate similar plots. We proceed by evaluating the dimensionality of the strange attractors.

The Lyapunov dimension $d_L$ may be estimated according to Kaplan and Yorke[7,8] from

$$d_L = j + \frac{\sum_{i=1}^{d} \lambda_i}{|\lambda_{j+1}|} \ , \tag{5.7}$$

where the integer $j$ is determined from the conditions

$$\sum_{i=1}^{j} \lambda_i \geq 0, \quad \sum_{i=1}^{j+1} \lambda_i < 0 \ . \tag{5.8}$$

The results for $d_L$ are also listed in Tables II and III. It has been argued that the dimensionality loss of the

phase-space attractors with respect to the equilibrium system [for which $d_L(0)=M$] is approximately given by

$$\Delta d_L \equiv d_L(\mathbf{F}_e)-d_L(0)\approx \dot{S}/k\lambda_{max} , \qquad (5.9)$$

where

$$S = -k\int d\Gamma f(\Gamma,t)\ln f(\Gamma,t) \qquad (5.10)$$

is the information theory entropy. $\dot{S}$ is the rate of irreversible entropy production and may be easily calculated,[35,22]

$$\dot{S}/k = -\int d\Gamma \ln f \frac{\partial f}{\partial t}$$

$$= -\int d\Gamma \ln f\left[-\frac{\partial}{\partial\Gamma}\cdot(f\dot{\Gamma})\right]$$

$$= -\int d\Gamma \,\dot{\Gamma}\cdot\frac{\partial f}{\partial\Gamma}=\int d\Gamma f\frac{\partial}{\partial\Gamma}\cdot\dot{\Gamma}=\langle\Lambda\rangle . \qquad (5.11)$$

The first step follows from the normalization of $f$, the second from inserting the Liouville equation (4.4). The final steps follow from partial integration and the use of (5.4). We conclude that

$$\Delta d_L \approx \sum\lambda/\lambda_{max} . \qquad (5.12)$$

This prediction is verified by our numerical results for not too large external fields $F_e \leq 2$. Obviously the dimensionality loss is an extensive quantity and persists in the thermodynamic limit.

The fact that nonequilibrium systems quickly collapse onto a fractal subspace of the complete equilibrium phase space with an associated loss in dimensionality is a general phenomenon. In addition to the problems mentioned previously it has been observed also by Morriss in a study of planar two-body shear flow.[36,37]

The consequences of this important result with respect to the second law of thermodynamics has been established very recently:[31,32,34] Only trajectories which on

the average convert heat into work and which are characterized by a negative friction $\langle\zeta\rangle$ (or $\langle\zeta_G\rangle$) will violate the second law. In view of the time-reversal invariance of the Nosé-Hoover or Gauss equations of motion (1.9) and (1.6), respectively, these trajectories must be precisely on the associated repellor and must be propagated backward in time. The repellor states are obtained from the strange attractor by the time-reversal transformation $q\rightarrow q$, $p\rightarrow -p$, $\zeta\rightarrow -\zeta$ (or $\zeta_G\rightarrow -\zeta_G$) and consequently form again a fractal object with a dimensionality $d_L$ less than the complete phase-space dimension $M$. Since time-reversal also means a sign change for the Lyapunov exponents the repellor states are characterized by a positive sum of Lyapunov exponents and a positive phase-space compressibility $\langle\Lambda\rangle$. It follows that the repellor is unstable: The slightest deviation will blow up very quickly and the trajectory will end up on the attractor again. One concludes (a) that an *exact* localization of the repellor is impossible because of its vanishing phase-space volume and (b) that any *approximate* effort to localize and follow a time-reversed trajectory on the repellor is impossible because of its inherent instability. Thus trajectories violating the second law do not occur in spite of the time reversal invariance of the equations of motion. Nosé-Hoover mechanics (1.9)—including Gauss's isokinetic equations (1.6) as a special case—therefore resolves the famous reversibility paradox first stated by Loschmidt in 1876 (Ref. 38) and discussed further by Boltzmann[39] for the special case of nonequilibrium steady or periodically varying states.

TABLE IV. Parameters for the isokinetic 32-body simulations with comoving "moving-frame" thermostats for various external fields $F_e$. All quantities are given in reduced units and are explained in Tables I and II and the Appendix.

| $F_e$ | 0.0 | 1.0 | 2.0 | 3.0 |
|---|---|---|---|---|
| $V$ | 64.0 | 64.0 | 64.0 | 64.0 |
| $kT$ | 1.00 | 1.02 | 1.08 | 1.31 |
| $k\tilde{T}$ | 1.00 | 1.00 | 1.00 | 1.00 |
| $\tilde{K}_0$ | 48.0 | 48.0 | 48.0 | 48.0 |
| $\langle\Phi\rangle$ | 8.9 | 9.1 | 9.2 | 9.9 |
| $t_{max}$ | 10.0 | 9.5 | 16.0 | 11.0 |
| $\alpha$ | 0.654 | | | |
| $\beta$ | 0.382 | | | |
| $\nu_D$ | 3.40 | | | |
| $\lambda_{max}$ | 3.70 | 3.69 | 3.64 | 3.54 |
| $h_K$ | 246 | 239 | 226 | 207 |
| $\sum\lambda$ | 0 | −9.0 | −28.1 | −88.3 |
| $\langle\Lambda\rangle$ | 0 | −7.8 | −28.5 | −88.0 |
| $d_L$ | 186.0 | 183.6 | 178.6 | 164.4 |
| $\kappa$ | | 0.124±0.010 | 0.144±0.010 | 0.155±0.010 |

computer time by the Prozessrechenanlage Physik of the University of Vienna. The National Science Foundation furnished generous travel support.

## APPENDIX

We should emphasize that the definition of "temperature" in a nonequilibrium system is not unambiguous. Strong one-dimensional shock waves have distinct longitudinal, transverse, nuclear, electronic, and radiation temperatures. Any definition must be clear and must reduce to the equilibrium one at equilibrium. In our system with two moving currents one can imagine two alternative definitions. The first, which we use in this paper, bases $T$ on the mean squared velocity $\mathbf{v} = \mathbf{p}/m$ relative to a fixed laboratory frame ($\mathbf{v}_L = 0$),

$$3kT = \langle m(\mathbf{v} - \mathbf{v}_L)^2 \rangle \tag{A1}$$

An alternative, favored by other authors, uses two separate thermometers. These move with velocity $\mathbf{u} = \langle \mathbf{J} \rangle / N$ either in the direction of the external force $\mathbf{F}_e$ (for particles with $c = +1$) or in the opposite direction ($c = -1$) and detect only the velocities of the appropriate comoving subset of particles. Assuming steady-state conditions this "current"-temperature $\widetilde{T}$ is

$$3k\widetilde{T} = \frac{1}{N} \sum_{i=1}^{N} m(\mathbf{v}_i - c_i\mathbf{u})^2$$

$$= 3kT - m\mathbf{u}^2 = 3kT - m\frac{(\kappa\mathbf{F}_e)^2}{(N/V)^2} . \tag{A2}$$

$\widetilde{T}$ is also included in Tables II and III. Our constraint equations of motion (1.7) are designed to control the "laboratory" temperature $T$. Methods of incorporating comoving thermostats into the equations of motion have been discussed by Evans and co-workers.[40,41]

To investigate the effect of the moving-frame thermostat on the Lyapunov spectrum, we have carried out a series of simulations for the 32-particle system using a moving-frame Gaussian thermodstat with fixed temperature $\widetilde{T}$. Instead of (1.6)–(1.8) the equations of motion are[41]

$$\dot{\mathbf{q}} = \frac{\mathbf{p}}{m} ,$$
$$\dot{\mathbf{p}} = \mathbf{F}(\mathbf{q}) - \widetilde{\zeta}_G \cdot \widetilde{\mathbf{p}} , \tag{A3}$$

where the Gaussian friction coefficient $\widetilde{\zeta}_G$ is given by

$$\widetilde{\zeta}_G = \frac{\dfrac{1}{m}\sum \widetilde{\mathbf{F}}(\mathbf{q})\cdot\widetilde{\mathbf{p}}}{\dfrac{1}{m}\sum \widetilde{\mathbf{p}}\cdot\widetilde{\mathbf{p}}} . \tag{A4}$$
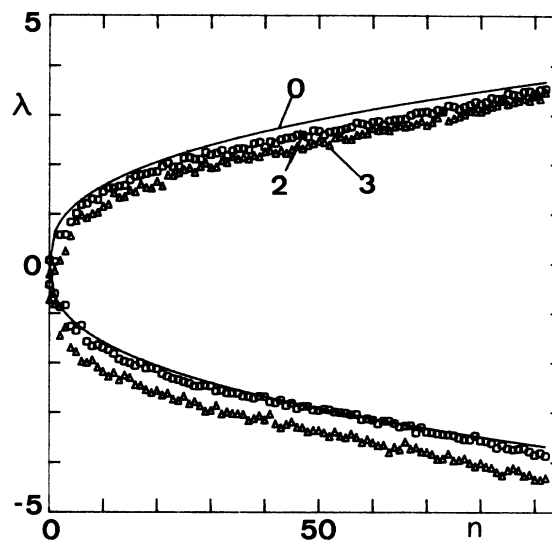


FIG. 6. Full Lyapunov spectra for an isokinetic 32-body fluid with comoving "moving-frame" thermostats for various reduced external fields $F_e$, as indicated by the labels. The simulation results are shown as symbols. The solid curve is a fit of (4.1) to the positive exponents for the equilibrium case ($F_e = 0$). All quantities are in reduced units.

Here,

$$\widetilde{\mathbf{p}} = \mathbf{p} - \frac{2}{N}\sum{}'\mathbf{p} \tag{A5}$$

is the momentum of a particle relative to the center of mass of the comoving subset of $N/2$ particles [over which the sum $\sum'$ in (A5) has to be performed]. Similarly,

$$\widetilde{\mathbf{F}}(\mathbf{q}) = \mathbf{F}(\mathbf{q}) - \frac{2}{N}\sum{}'(\mathbf{F}(\mathbf{q})\cdot\hat{\mathbf{x}})\hat{\mathbf{x}} , \tag{A6}$$

where $\hat{\mathbf{x}}$ is a unit vector in the direction of the external field $\mathbf{F}_e$. For the constant temperature $\widetilde{T}$ we have

$$2\widetilde{K}_0 = 3Nk\widetilde{T} = \frac{1}{m}\sum\widetilde{\mathbf{p}}\cdot\widetilde{\mathbf{p}} . \tag{A7}$$

Our results are summarized in Table IV and Fig. 6 and confirm all our conclusions reached with the fixed-frame laboratory thermostat in Secs. IV and V. The only new feature is that the branch of negative Lyapunov exponents for the largest external field $\mathbf{F}_e = 3$ is shifted more strongly to more negative values than the positive branch.

[1]R. H. G. Helleman, *Fundamental Problems in Statistical Mechanics V*, edited by E. G. D. Cohen (North-Holland, Amsterdam, 1980), p. 165.

[2]A. Wolf, J. B. Swift, H. L. Swinney, and J. A. Vastano, Physica, D **16**, 285 (1985).

[3]J.-P. Eckmann and D. Ruelle, Rev. Mod. Phys. **57**, 617 (1985);

addendum: **57**, 1115 (1985).

[4]G. Benettin, L. Galgani, and J.-M. Strelcyn, Phys. Rev. A **14**, 2338 (1976).

[5]I. Shimada and T. Nagashima, Prog. Theor. Phys. **61**, 1605 (1979).

[6]A. J. Lichtenberg and M. A. Lieberman, *Regular and Stochas-*

*tic Motion* (Springer, New York, 1983).

[7]J. Kaplan and J. Yorke, in *Functional Differential Equations and the Approximation of Fixed Points,* Vol. 730 of *Lecture Notes in Mathematics,* edited by H. O. Peitgen and H. O. Walther (Springer-Verlag, Berlin, 1978).

[8]P. Frederikson, J. Kaplan, E. Yorke, and J. Yorke, J. Differ. Equ. **49**, 185 (1983).

[9]H. Mori, Prog. Theor. Phys. **63**, 1044 (1980).

[10]W. G. Hoover, H. A. Posch, and S. Bestiale, J. Chem. Phys. **87**, 6665 (1987).

[11]W. G. Hoover and H. A. Posch, Phys. Lett. A **123**, 227 (1987).

[12]D. J. Evans, W. G. Hoover, B. H. Failor, B. Moran, and A. J. C. Ladd, Phys. Rev. A **28**, 1016 (1983).

[13]D. J. Evans and W. G. Hoover, Ann. Rev. Fluid Mech. **18**, 243 (1986).

[14]W. G. Hoover, in *Molecular Dynamics,* Vol. 258 of *Lecture Notes in Physics* (Springer-Verlag, Berlin, 1986).

[15]S. Nosé, Mol. Phys. **52**, 255 (1984).

[16]S. Nosé, J. Chem. Phys. **81**, 511 (1984).

[17]S. Nosé, Mol. Phys. **57**, 187 (1986).

[18]W. G. Hoover, Phys. Rev. A **31**, 1695 (1985).

[19]D. J. Evans and B. L. Holian, J. Chem. Phys. **83**, 4069 (1985).

[20]H. A. Posch, W. G. Hoover, and F. J. Vesely, Phys. Rev. A **33**, 4253 (1986).

[21]B. L. Holian and W. G. Hoover, Phys. Rev. A **34**, 4229 (1986).

[22]B. L. Holian, Phys. Rev. A **34**, 4238 (1986).

[23]G. Benettin, L. Galgani, A. Giorgilli, and J. M. Strelcyn, C. R. Acad. Sci. (Paris) **286A**, 431 (1978).

[24]G. Benettin, L. Galgani, A. Giorgilli, and J. M. Strelcyn, Meccanica **15**, 9 (1980).

[25]W. G. Hoover and H. A. Posch, Phys. Lett. A **113**, 82 (1985).

[26]I. Goldhirsch, P.-L. Sulem, and S. A. Orszag, Physica D **27**, 311 (1987).

[27]R. P. Feynman and H. Kleinert, Phys. Rev. A **34**, 5080 (1986).

[28]A. A. Maradudin, E. W. Montroll, and G. H. Weiss, *Theory of Lattice Dynamics in the Harmonic Approximation* (Academic, New York, 1963).

[29]B. L. Holian and D. J. Evans, J. Chem. Phys. **83**, 3560 (1985).

[30]Ja. B. Pesin, Usp. Mat. Nauk **32**(4), 55 (1977) [Russ. Math. Surv. **32**(4), 55 (1977)].

[31]B. L. Holian, W. G. Hoover, and H. A. Posch, Phys. Rev. Lett. **59**, 10 (1987).

[32]W. G. Hoover, Phys. Rev. A **37**, 252 (1988).

[33]B. Moran, W. G. Hoover, and S. Bestiale, J. Stat. Phys. **48**, 709 (1987).

[34]W. G. Hoover, H. A. Posch, B. L. Holian, M. J. Gillan, M. Mareschal, and C. Massobrio, Mol. Simul. **1**, 79 (1987).

[35]D. J. Evans, Phys. Rev. A **32**, 2923 (1985).

[36]G. P. Morriss, Phys. Lett. A **122**, 236 (1987).

[37]G. P. Morriss (unpublished).

[38]J. Loschmidt, Sitzungsber. kais. Akad. Wiss. Wien, 2. Abt. **73**, 128 (1876).

[39]L. Boltzmann, Sitzungsber. kais. Akad. Wiss. Wien, 2. Abt. **75**, 67 (1877); English translation, S. G. Brush, *Kinetic Theory, Vol. 2, Irreversible Processes* (Pergamon, Oxford, 1966), p. 188.

[40]D. J. Evans and G. P. Morriss, Phys. Rev. Lett. **56**, 2172 (1986).

[41]D. MacGowan and D. J. Evans, Phys. Rev. A **34**, 2133 (1986).